Possibility of ^{14}C cluster as a building block of medium-mass nuclei

N. Itagaki, A. V. Afanasjev, and D. Ray

Phys. Rev. C **101**, 034304 — Published 12 March 2020

DOI: 10.1103/PhysRevC.101.034304

The possibility of ^{14}C cluster as a building block of medium mass nuclei

N. Itagaki,[1] A. V. Afanasjev,[1,2] and D. Ray[3]

[1] *Yukawa Institute for Theoretical Physics, Kyoto University, Kitashirakawa Oiwake-Cho, Kyoto 606-8502, Japan*

[2] *Department of Physics and Astronomy, Mississippi State University, MS 39762, USA*

[3] *Institute for Systems Engineering Research (ISER), Mississippi State University, MS 39762, USA*

(Dated: February 11, 2020)

The possibility of the ^{14}C cluster being a basic building block of medium mass nuclei is discussed. Although α cluster structures have been widely discussed in the light $N \approx Z$ mass region, the neutron to proton ratio deviates from unity in the nuclei near β-stability line and in neutron-rich nuclei. Thus, more neutron-rich objects with $N > Z$ could become the building blocks of cluster structures in such nuclei. The ^{14}C nucleus is strongly bound and can be regarded as such a candidate. In addition, the path to the lowest shell-model configuration at short relative distances is closed for the ^{14}C+^{14}C structure contrary to the case of the ^{12}C+^{12}C structure; this allows to keep appreciable separation distance between the ^{14}C clusters. The recent development of antisymmetrized quasi-cluster model (AQCM) allows us to utilize jj-coupling shell model wave function for each cluster in a simplified way. The AQCM results for the ^{14}C+^{14}C structure in ^{28}Mg are compared with the ones of cranked relativistic mean field (CRMF) calculations. Although theoretical frameworks of these two models are quite different, they give similar results for the nucleonic densities and rotational properties of the structure under investigation. The existence of linear chain three ^{14}C cluster structure in ^{42}Ar has also been predicted in AQCM. These results confirm the role of the ^{14}C cluster as a possible building block of cluster structures in medium mass nuclei.

I. INTRODUCTION

The α cluster structures have been extensively studied over the years [1, 2]. Since the binding energy per nucleon is extremely large in ^{4}He, it can be a building block of the nuclear systems called α cluster. Also, the relative interaction between the α clusters is weak, which is another condition for the appearance of the cluster structures. For example, ^{8}Be is not bound but its ground state has a developed α+α cluster structure. The candidates for α cluster states have been widely discussed in other light $4N$ (N is integer here) nuclei [3]. This is illustrated by a few examples below. The second 0^+ state of ^{12}C at $E_x = 7.65$ MeV, located just above the threshold energy to the decay into three α's, has a developed three-α cluster structure and plays a crucial role in the formation of ^{12}C in stars [4]. In ^{16}O, the first excited state at $E_x = 6.05$ MeV, located very close to the threshold of the decay into ^{12}C and ^{4}He, can be interpreted as ^{12}C+^{4}He cluster state. It has been known as the mysterious 0^+ state; the reproduction of this state based on the standard picture (shell-model approaches) is still a big challenge. Various cluster structures have been proposed also in ^{20}Ne, ^{24}Mg, and ^{44}Ti etc. [1–3].

The description of such cluster structures has been attempted in simple cluster models. However, it is well known that non-central nuclear interactions are very important in nuclear systems and their effects cannot be taken into account in simple α cluster models. With increasing mass number, the symmetry of the jj-coupling shell model dominates the nuclear structure, and subclosure configurations of j-shells, $f_{7/2}$, $g_{9/2}$, and $h_{11/2}$ become important, corresponding to the magic numbers of 28, 50, and 126 [5]. Indeed the observation of these magic numbers is the evidence that the spin-orbit interaction strongly contributes in the medium and heavy mass regions, and this interaction is known to play a substantial role in breaking the α clusters [6].

Therefore, it is natural to think about a different object as a cluster in the study of medium mass nuclei. Here one should also consider that neutron to proton ratio of stable nuclei deviates from unity with increasing mass number. Thus, there is the possibility that more neutron-rich object could be a building block of cluster structures. In this study, we discuss the possibility that the ^{14}C nucleus could be a cluster. This can be justified by the following arguments.

First of all, ^{14}C is strongly bound. This is because the proton number 6 corresponds to the subclosure of the $p_{3/2}$ subshell of the jj-coupling shell model, and the neutron number 8 is the magic number corresponding to the closure of the p shell. Although ^{14}C has two valence neutrons, the lowest threshold to emit particle is the neutron threshold at $E_x = 8.18$ MeV, which is high enough value. In addition, because of strong shell effects, there is no excited state below $E_x = 6$ MeV just like in ^{16}O. The β-decay of free ^{14}C is very slow reflecting the stability of this nucleus. Thus, ^{14}C is a famous nucleus used for the age determination [7]. The second argument is the following: although the single ^{14}C nucleus is β-unstable, the line connecting the origin of the nuclear landscape and the point of 6 protons and 8 neutrons (corresponding to ^{14}C) on the nuclear chart, which has $N/Z \sim 1.3$, extrapolates into β-stability line above $Z \approx 40$. The third argument is that it is well known that ^{14}C is emitted from some of heavy nuclei [such as $^{221-224,226}$Ra, ^{223,225}Ac and ^{221}Fr (see Ref. [8])] in the process which is called cluster decay [9]. In reality, there is much more experimental

data for the ^{14}C emission as compared with the emission of ^{12}C in medium and heavy mass nuclei, and neutron richness of ^{14}C can be important for that. These experimental data also strongly suggest that ^{14}C can be a building block of cluster structures in heavy nuclei. The fourth argument is that the candidates for the ^{14}C cluster structures have already been discussed in the Oxygen isotopes [10–13]. The first excited state of ^{16}O is known as mysterious state the interpretation of which involves the ^{12}C+α cluster structure [14]. In a similar fashion, the interpretation of some of the states in the ^{18}O and ^{19}O nuclei is based on possible ^{14}C+α cluster structure [10–13]. Finally, contrary to the case of the ^{12}C+^{12}C cluster structure, the path to the lowest shell-model configuration is closed at short relative distances in the ^{14}C+^{14}C cluster structure. This factor leads to appreciable distance between the ^{14}C clusters and it is a subject of the present study.

In this article, the appearance of ^{14}C cluster structures is investigated within the framework of two theoretical approaches. One of them is antisymmetrized quasi-cluster model (AQCM) [15] and another is covariant density functional theory (CDFT) [16]. The details of these two approaches are discussed and their applicabilities to the study of clusters states are examplified in Secs. II and III, respectively. By definition, the cluster states appear in the cluster models and AQCM is one of their representatives. However, to prove the possibility of the existence of such a state, it is important to show the possibility of its appearance also in a more general framework capable to include both shell model and cluster states simultaneously. And CDFT framework is used here as such an alternative. Note that at present relativistic (covariant) and non-relativistic DFT approaches are only approaches capable to describe physical phenomena across the whole nuclear chart. The clustering is not assumed in the DFT approaches. However, the appearance of cluster states in the DFT approaches, which are similar in properties to those obtained in cluster models, gives an additional confidence in the possibility of the existence of such exotic states.

There are also additional factors which call for a comparative and complimentary study based on two different theoretical frameworks. First, both types of approaches still rely on some phenomenological input. As a result, it is important to outline the possible range of predictions. Second, extremely limited spectroscopic experimental data on clusterization in the $A > 20$ nuclei does not allow to discriminate existing differences in the predictions of the properties of cluster states obtained with cluster and DFT type models (see Ref. [17]). As a consequence, it is difficult to give quantifiable preference for the predictions of one or another model.

This paper is organized as follows. The ^{14}C+^{14}C cluster structure of ^{28}Mg is investigated by the AQCM and CRMF approach in Secs. II and III, respectively. In Sec. IV, the possibility of the linear chain configuration of three ^{14}C clusters in ^{42}Ar is studied for the first time. The structure of the ^{14}C nucleus and of the ground state of ^{28}Mg are discussed within AQCM in Secs. V and VI, respectively. The conclusions are presented in Sec. VII.

II. THE ^{14}C+^{14}C CLUSTER STRUCTURE IN ^{28}MG WITHIN THE ANTISYMMETRIZED QUASI-CLUSTER MODEL.

We start our analysis from the consideration of the ^{14}C cluster structures in ^{28}Mg within the framework of the antisymmetrized quasi-cluster model. The protons of ^{14}C correspond to the subclosure of $p_{3/2}$ in the jj-coupling shell model. The jj-coupling shell model wave functions can be easily prepared starting from the cluster model. Indeed, the AQCM proposed in Refs. [15, 18–27] allows smooth transformation of the α cluster model wave functions to the jj-coupling shell model ones and the incorporation of the effects of the spin-orbit interaction. A reliable nucleon-nucleon interaction, which includes both the cluster and shell features in the light and medium mass nuclei, is inevitably needed. The Tohsaki interaction, which has finite range three-body terms [15, 27–29], is employed here. Although this is a phenomenological interaction, it provides a reasonable size and binding energy for the α cluster and reproduces α+α scattering phase shifts. In addition, it describes the saturation properties of nuclear matter rather well.

In AQCM, each single-particle wave function is described by a Gaussian,

$$\phi = \left(\frac{2\nu}{\pi}\right)^{\frac{3}{4}} \exp\left[-\nu\left(\boldsymbol{r}-\boldsymbol{\zeta}\right)^2\right]\chi, \tag{1}$$

where the Gaussian center parameter $\boldsymbol{\zeta}$ shows the expectation value of the position of the particle, and χ is the spin-isospin wave function. The size parameter ν is set to 0.17 fm^{-2} for ^{28}Mg (two ^{14}C) and ^{42}Ar (three ^{14}C). This is the parameter which determines the Gaussian width of the single-particle wave function. It is known that the value of $\nu \sim 0.25$ fm^{-2} gives the observed radius of ^{4}He, and, in addition, the employed interaction is designed to give the optimal energy of the α cluster with this value. However, it is also known that the optimal size parameter changes with increasing mass number. Note that such a situation is common in the shell model analyses and that ν of AQCM is directly related to $\hbar\omega$ of the shell model. Since the saturation density of the medium and heavy mass nuclear systems differs significantly from the central density of the ^{4}He nucleus (see Fig. 2.4 in Ref. [30]), the ν value should be mass dependent and chosen properly. The main focus of the present article is the ^{28}Mg nucleus; thus we use $\nu = 0.17$ fm^{-2} which provides a reasonable central density for this nucleus.

The Slater determinant in the conventional Brink model [1] is constructed from these single particle wave functions by antisymmetrizing them. Here, four single particle wave functions with different spin and isospin

sharing a common Gaussian center parameter $\boldsymbol{\zeta}$ correspond to an α cluster. In the conventional cluster models, there is no spin-orbit effect for the α clusters. Thus, they are changed into quasi-clusters based on AQCM [15, 18–26]. According to AQCM, when the original position of one of the particles (the value of Gaussian center parameter) is $\boldsymbol{R}$, the Gaussian center parameter of this nucleon is transformed by adding the imaginary part as

$$\boldsymbol{\zeta} = \boldsymbol{R} + i\Lambda \boldsymbol{e}^{\rm spin} \times \boldsymbol{R}, \tag{2}$$

where $\boldsymbol{e}^{\rm spin}$ is a unit vector for the intrinsic-spin orientation of this nucleon. It has been previously shown that the lowest configurations of the jj-coupling shell model can be achieved by $\Lambda = 1$ and $\boldsymbol{R} \to 0$ for all the nucleons [23].

For the description of ^{14}C, at first, di-nucleon clusters are prepared; in each di-nucleon cluster, two nucleons with opposite spin and same isospin are sharing common Gaussian center parameters. Four di-nucleon clusters with a tetrahedron configuration (the distance between two di-neutron clusters is parameterized as R) and small relative distances ($R \to 0$) corresponds to the closure of the p-shell, which is introduced for the neutron part. In the calculations, R is set to 0.1 fm. For the proton part, three di-proton clusters with equilateral triangular configuration and small distance between them are introduced, and the imaginary parts of the Gaussian center parameters are given as $\Lambda = 1$ in Eq. (2), which correspond to the subclosure of the $p_{3/2}$ shell [15, 22].

For the analysis based on AQCM, the Hamiltonian consists of kinetic energy and potential energy terms, and the potential energy has central, spin-orbit, and Coulomb parts. For the central part, the Tohsaki interaction [28] is adopted, which has finite range three-body nucleon-nucleon interaction terms in addition to two-body terms. This interaction is designed to reproduce both saturation properties and scattering phase shifts of two α clusters. For the spin-orbit part, the spin-orbit term of the G3RS interaction [31], which is a realistic interaction originally developed to reproduce the nucleon-nucleon scattering phase shifts, is adopted. The combination of these two has been investigated in detail in Refs. [26, 27].

We start the discussion with the comparison of the ^{12}C+^{12}C and ^{14}C+^{14}C systems. The energy curves of the 0^+ states of these two systems are shown in Fig. 1. It is confirmed that in the case of the ^{12}C+^{12}C system (dotted line), the optimal distance is rather small, around 2 fm. According to the jj-coupling shell model, the small distance limit of two ^{12}C corresponds to the lowest configuration of ^{24}Mg. This means that the path going to the ground state after the fusion is opened for the ^{12}C+^{12}C system. This situation is different in the case of ^{14}C+^{14}C system (solid line). Small distance limit of two ^{14}C does not correspond to the lowest jj-coupling shell model wave function of ^{28}Mg. As a result, the minimum energy appears around the relative distance of approximately 3.5 fm. This result suggests the possibility that ^{14}C clusters keep the relative distance, which is much larger than in the case of the ^{12}C+^{12}C system, and form a cluster structure. The dashed line is for the energy of the ^{16}O+^{16}O system, and again the path going to the ground state is closed. In this case, in addition to this closed path effect, the large Coulomb repulsion acts in favor of the appearance of well developed cluster structure (the optimal relative distance of which is around 5 fm). The ^{16}O+^{16}O structure of ^{32}S has been discussed for years [32], but it has been known that the ^{16}O+^{16}O cluster component corresponds to highly excited states above the Coulomb barrier [33]. The possibility of the existence of highly excited superdeformed bands in ^{32}S based on the ^{16}O+^{16}O structure has also been discussed in density functional theories [34–36]. In the case of ^{14}C+^{14}C system, the

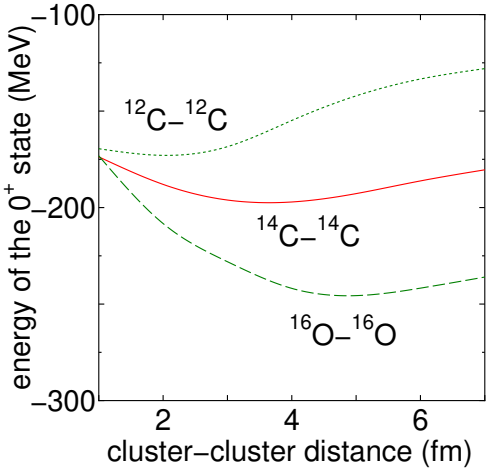

FIG. 1. The 0^+ energy curves of ^{12}C+^{12}C (^{24}Mg, dotted line) and ^{14}C+^{14}C (^{28}Mg, solid line). The dashed curve corresponds to the 0^+ energy curve of ^{16}O+^{16}O (^{32}S).

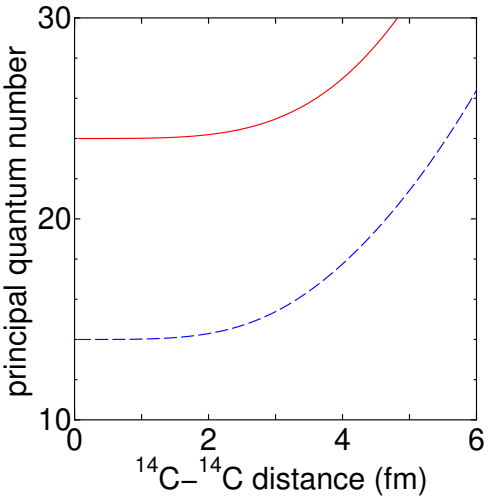

FIG. 2. The expectation value of the principal quantum number n of the harmonic oscillator for the 0^+ state of the ^{14}C+^{14}C configuration in ^{28}Mg as a function of relative distance. The solid (red) line is for the neutrons, whereas the dashed line (blue) is for the protons.

state appears around the threshold because of smaller Coulomb repulsion.

One can see that the ^{14}C+^{14}C configuration does not have the path to the ground state configuration of ^{28}Mg by calculating the principal quantum number n of the harmonic oscillator. The expectation values of the proton and neutron n for the 0^+ state of the ^{14}C+^{14}C configuration (^{28}Mg) are shown in Fig. 2 as a function of relative distance. The proton n value converges to 14 at small distance between the two ^{14}C clusters. This is the lowest principal quantum number for 12 protons. Thus, the path to the lowest shell-model configuration (2 protons are in the lowest s-shell, 6 protons in the p-shell, and 4 protons in the sd-shell) is open for the proton subsystem. As compared with proton subsystem, there are four additional neutrons in the neutron subsystem of ^{28}Mg. As a consequence, the lowest principal quantum number increases to 22 because four additional neutrons are located in the sd-shell ($4\times2=8$). However, the solid line in Fig. 2 converges to 24 at small distance between the two ^{14}C clusters. This means that the ^{14}C+^{14}C configuration in ^{28}Mg is located at two $\hbar\omega$ excitation energy with respect of the lowest shell-model configuration in this nucleus. This feature appears also in the CRMF calculations (see next section). Note that similar situation to above discussed exists also in the proton and neutron subsystems of the ^{12}C+^{12}C cluster structure of ^{24}Mg.

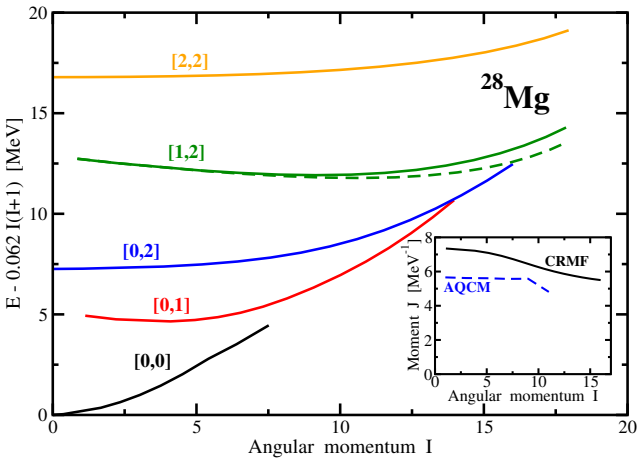

FIG. 3. Excitation energies of calculated CRMF configurations in ^{28}Mg relative to a rotating liquid drop reference $AI(I+1)$, with the inertia parameter $A=0.062$. The insert shows the moments of inertia of the ^{14}C+^{14}C cluster structure as a function of the spin.

III. THE ^{28}MG NUCLEUS WITHIN THE CRANKING RELATIVISTIC MEAN FIELDS APPROACH

An alternative way to look on clustering in nuclei is through the prism of density functional theories (DFT). Both relativistic and non-relativistic DFTs have been applied to the investigation of this phenomenon in nuclei (see Refs. [36, 37] and references quoted therein). The advantage of the DFT framework is the fact that it does not assume the existence of cluster structures; the formation of cluster structures proceeds from microscopic single-nucleon degrees of freedom via many-body correlations [37–40]. As a result, the DFT framework allows the simultaneous treatment of cluster and mean-field-type states.

The covariant (relativistic) DFT (CDFT) framework is employed in the present article. In the CDFT approach the nucleus is described as a system of pointlike nucleons, Dirac spinors, coupled to mesons and to the photons (see Ref. [16]). The nucleons interact by the exchange of several mesons, namely, a scalar meson σ and three vector particles, ω, ρ and the photon. The CDFT approach provides reasonably accurate global description of the ground states properties [41]; in particular, their experimental charge radii, sensitive to the density distributions of occupied single-particle orbitals, are described with the precision better than 0.5% [42]. Also experimentally observed superdeformed (SD) structures, characterized by highly elongated shapes, are described with high accuracy across the nuclear chart starting from the SD band in ^{40}Ca [43] and ending by extensive regions of superdeformation with $A\sim150$ [44] and $A\sim190$ [45]. Different aspects of clusterization at low spins have been studied in its framework in Refs. [37, 39, 46–50]. The clusterization effects have also been studied in rotating nuclei. For example, "rod-shaped" structures built of three and four α-clusters have been investigated within the cranked relativistic mean field theory (CRMF) (which is the version of the CDFT for rotating nuclei, see Ref. [16]) in ^{12}C [51] and ^{16}O [52], respectively. The clusterization features in some configurations of rotating higher mass nuclei have been investigated in the CRMF approach in Refs. [36, 40][1].

This is a reason why cranked relativistic mean field (CRMF) approach is also used in the present manuscript for the study of clusterization in ^{28}Mg. The CRMF calculations are performed with the NL3* covariant energy density functional (CEDF) [56].

Figure 3 shows calculated energies of the lowest configurations in ^{28}Mg. The configurations are labeled by

[1] The clusterization effects in some configurations of rotating nuclei have also been investigated in non-relativistic DFTs based on Skyrme functionals. For example, "rod-shaped" structures built on multiple number of α-clusters have been studied in cranked Skyrme HF approaches in even-even $N=Z$ nuclei from ^{12}C up to ^{32}S in Refs. [53–55]. In addition, the investigation of other types of clusterization in heavier nuclei has been carried out in this framework in Ref. [35]. The similarity of many results obtained in the relativistic and non-relativistic DFTs to those obtained in cluster type models clearly indicates the applicability of the DFT approaches to the description of clusterization phenomena.

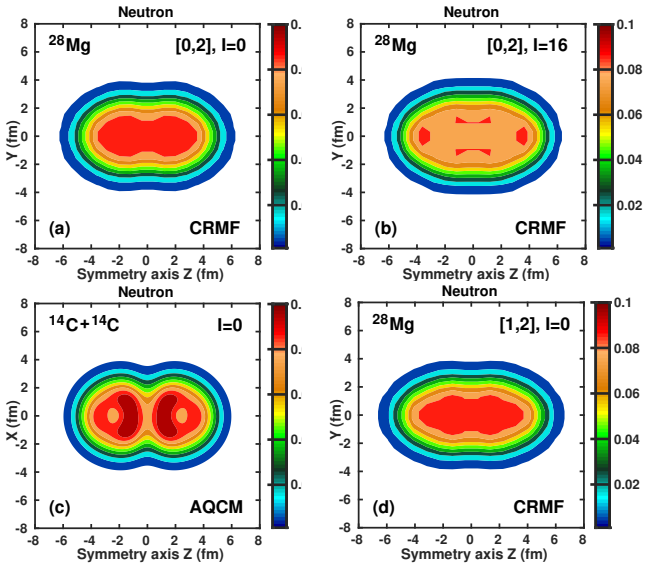

FIG. 4. Neutron density distributions of the configurations of interest. Panels (a), (b) and (d) show the densities of the [0,2] and [1,2] configurations obtained in the CRMF calculations, while panel (c) the densities of the ^{14}C+^{14}C structure obtained in the AQCM calculations. The density colormap starts at $\rho = 0.005$ fm^{-3} and shows the densities in fm^{-3}.

shorthand $[p, n]$ labels where p (n) is the number of occupied $N = 3$ proton (neutron) intruder orbitals (here N is principal quantum number). The ground state band [0,0] has no such orbitals occupied and it has quadrupole deformation of $\beta_2 = 0.34$ at spin $I = 0$. As discussed in Ref. [36], such normal deformed band has limited angular momentum content and it terminates in purely single-particle state at $I = 8$. Subsequent particle-hole excitations lead to rotational bands with structure [0,1], [0,2], [1,2], [2,2], ..., which have larger angular momentum content (see Fig. 3) and larger deformation. Neutron densities of selected states of these rotational bands are shown in Fig. 4.

Of particular interest is the [0,2] configuration and especially its relative properties with respect of the ground state [0,0] configuration. This is because the transition from the [0,0] configuration to the [0,2] configuration involves the excitation of two neutrons between two major shells with principal quantum numbers $N = 2$ and $N = 3$ while the protons are not affected by such type of excitations. This is equivalent to the situation in the AQCM calculations (see Sec. II) in which the ^{14}C+^{14}C cluster structure in ^{28}Mg is located at two $\hbar\omega$ excitation energy (generated in neutron subsystem) with respect of the lowest shell-model configuration. The density distribution of the [0,2] configuration at spin $I = 0$ (Fig. 4 (a)) corresponds to the ^{14}C+^{14}C cluster structure and it is similar (especially in high-density region) to the one obtained in the AQCM calculations (Fig. 4 (c)). In both calculations, the ^{14}C+^{14}C distance is approximately equal to 4 fm.

Note that the attribution of the [0,2] configuration to the ^{14}C+^{14}C cluster structure is based not only on above mentioned arguments but also on relative properties of cluster structures in the ^{28}Mg, ^{28}Si and ^{32}S nuclei (see discussion in the end of this chapter) related to the impact of the occupation of specific single-particle orbitals on the clusterization phenomomen (see Refs. [40, 50]). In addition, one can define respective CRMF configuration by excluding the configurations which do not satisfy required conditions. For example, the [0,1] and [1,2] configurations have negative parity and represent the groups of four rotational bands with either non-existent or small signature splittings. Two of these bands in the group have odd spins. These features indicate active role of two particles located in different single-particle orbitals and they are inconsistent with the ^{14}C+^{14}C cluster structure. Only the [0,0], [0,2] and [2,2] configurations are represented by a single band of positive parity and even spins. However, the lowest in energy [0,0] configuration does not have sufficient deformation to form a cluster structure. Highly excited [2,2] configuration involves the excitation (with respect of the [0,0] configuration) of two neutrons and two protons between two major shells with principal quantum numbers $N = 2$ and $N = 3$. Thus, it is not consistent with the AQCM results.

Note that ^{14}C+^{14}C cluster structure behaves differently as a function of the spin in the CRMF and AQCM calculations. This is illustrated in the insert to Fig. 3 which shows the moments of inertia of the ^{14}C+^{14}C cluster structure as a function of the spin. In the CRMF calculations, the moment of inertia is gradually decreasing with spin. This is due to two factors: the decrease of quadrupole deformation and washing out of clusterization with increasing spin which is generally observed in DFTs calculations (see Refs. [36, 40]). The comparison of the densities at spins $I = 0$ and 16 illustrates the latter feature (see Figs. 4(a) and (b)). On the contrary, the moments of inertia are somewhat smaller in the AQCM calculations and they stay almost constant up to $I = 8$. Note that in AQCM it is assumed that cluster structure persists even at highest calculated spins. In the light of distinct predictions of these two models, the experimental observation of the superdeformed band built on the ^{14}C+^{14}C structure would be extremely useful for clarification of existing differences in the description of clusterization in the DFT and cluster-originating models.

Note that in the CRMF calculations the [0,2] configuration, representing the ^{14}C+^{14}C cluster structure, plays a role of a basic building block of more elongated cluster structures with the [1,2] configurations, which are created by means of particle-hole excitations. At spin zero, the total (proton + neutron) quadrupole deformations of the [0,2] and [1,2] configurations are 0.81 and 0.89, respectively. The density of the [1,2] configuration is shown in Fig. 4(d). The differences in the density distributions of the [0,2] and [1,2] configurations are due to proton particle-hole excitation from the 3/2[211] orbital into 1/2[330] one. These orbitals have different spatial distributions of the single-particle density (see

Ref. [40, 50] for details) and thus such a particle-hole excitation moves density from the middle part of the nucleus to the polar region leading to a more elongated shape (compare Fig. 4(d) with Fig. 4(a)). Note that there are two [1,2] configurations which are signature degenerated up to $I \sim 10$ because of the degeneracies of the $3/2[211](r = \pm i)$ orbitals. Subsequent particle-hole excitations, leading to the [2,2] configuration with quadrupole deformations of 1.13 at spin zero, partially suppress ^{14}C+^{14}C cluster structure and form ellipsoidal-like density distribution.

To shed additional light on these predictions and their differences it is important to compare cluster and mean field model predictions in neighboring nuclei. Fortunately, there are two nuclei, namely, ^{32}S and ^{28}Si for which such extensive comparisons are possible. The most interesting is the case of superdeformed states in the ^{28}Si nucleus for which some experimental data are available [57]. Based on the comparison of experimental and calculated moments of inertia presented in Ref. [58], the observed 4^+ and 6^+ superdeformed states in this nucleus are most likely associated with the [2,2] configuration. The calculated kinematic moment of inertia of this configuration $J^{(1)} \approx 6.68\hbar^2$/MeV, which is nearly constant for large spin range, is only slightly above experimental one ($J^{(1)} \approx 6\hbar^2$/MeV [57]). The density distribution of the [2,2] configuration clearly shows the clusterization into two equal segments (see Fig. 2c in Ref. [58]). The [2,2] configuration in ^{28}Si is closely connected with the [0,2] configuration in ^{28}Mg; it is built from the latter one by an addition of two protons (into the $1/2[330]$ orbital) and removal of two neutrons (from the $3/2[211]$ orbital) [see Fig. 2 in Ref. [40] for a representative single-particle routhian diagram]. Thus, the [2,2] configuration in ^{28}Si can be considered as the $(^{14}\mathrm{C} + \pi - \nu) \otimes (^{14}\mathrm{C} + \pi - \nu))$ cluster structure. Note that there are large similarities in the predictions of the properties of oblate, prolate and superdeformed bands obtained in the CRMF calculations [58] and those within the antisymmetrized molecular dynamics (AMD) model of Ref. [59]. In particular, the CRMF and AMD results for excitations energies and moments of inertia of superdeformed band in this nucleus are close to each other and they are not far away from experimental data of Ref. [57]. The calculated density distributions of the configurations assigned to this band are similar in shape in these two approaches; however, the CRMF calculations predict larger degree of clusterization as compared with the AMD ones (compare Fig. 2c in Ref. [58] with Fig. 2(c) in Ref. [59]).

Another interesting case is the superdeformed rotational band in ^{32}S which has been the subject of many studies in the cluster and mean field approaches. The wave function of this superdeformed band contains a significant admixture of the molecular ^{16}O+^{16}O structure [35, 60] but its weight depends on the model. For example, its weight is 57% in deformed-basis AMD calculations of Ref. [60] but it is smaller ($\approx 30\%$) in the calculations of Ref. [35]. In the CRMF calculations, it has

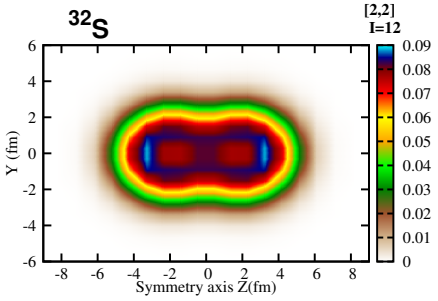

FIG. 5. Neutron density distributions of the [2,2] configuration in ^{32}S obtained in the CRMF calculations at spin $I = 12$.

the [2,2] configuration (see Ref. [36]) which is built from the [2,2] configuration of ^{28}Si by an addition of two protons and two neutrons into non-intruder $1/2[211]$ orbitals (see right panel of Fig. 2 in Ref. [40] for a single-particle routhian diagram). Note that there are large similarities between single-particle spectra of superdeformed configurations obtained in the CRMF and AMD+GCM calculations (compare right panel of Fig. 2 of Ref. [40] with Figs. 3 and 4 of Ref. [61]). The density distribution of the [2,2] configuration is presented in Fig. 5. One can see that it is built from two clusters separated by approximately 3.5 fm. Note that this clusterization becomes more pronounced at low spin. A peculiar feature of each cluster is the depression of the density in its central region which allows to attribute each of them to a somewhat deformed ^{16}O nucleus. This is because such a depression is also present in the ground state of spherical ^{16}O nucleus both in experiment and in theory (see experimental data in Fig. 3 of Ref. [62] and the results of the CDFT calculations in Fig. 1 of Ref. [63]). All these features suggest significant admixture of the molecular ^{16}O+^{16}O structure to the wave function of the [2,2] configuration obtained in the CRMF calculations.

IV. LINEAR CHAIN STRUCTURE ^{14}C+^{14}C+^{14}C IN ^{42}AR.

Next, we consider the case of linear chain structure of three ^{14}C clusters (^{14}C+^{14}C+^{14}C) in ^{42}Ar. The energy curves for such a structure are shown in Fig. 6 as a function of the ^{14}C+^{14}C distance. The AQCM solutions for the states with angular momentum ranging from $I = 0$ up to $I = 8$ are shown in this figure. Similar to the case of cluster ^{14}C+^{14}C structure in ^{28}Mg, the minima of the energy curves are obtained around the threshold energy with the relative distance of the ^{14}C clusters being approximately equal to $\sim$4 fm. The moment of inertia of the calculated rotational band is 15.59 MeV^{-1}. In the future, one should investigate the stability of the linear chain state against the bending motion. Even if it is not stable against the bending motion at spin zero, there is a possibility that it becomes stabilized when large angular

momentum is given to the system. This is because it is well known that rotation can stabilize elongated shapes owing to the centrifugal force [64–66].

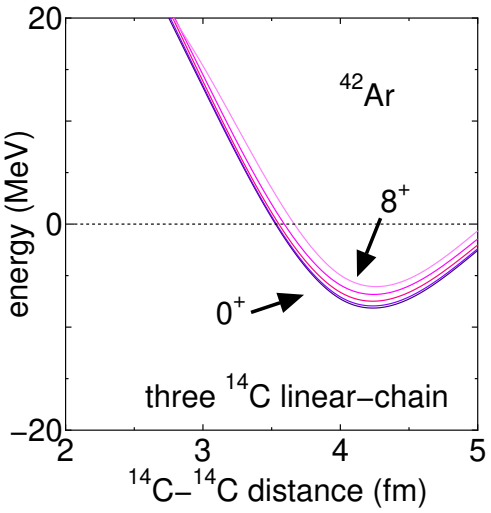

FIG. 6. The energy curves for the linear chain of three ^{14}C clusters (^{42}Ar) measured from the three ^{14}C threshold as a function of the ^{14}C-^{14}C distance. The angular momentum is changed from 0 to 8.

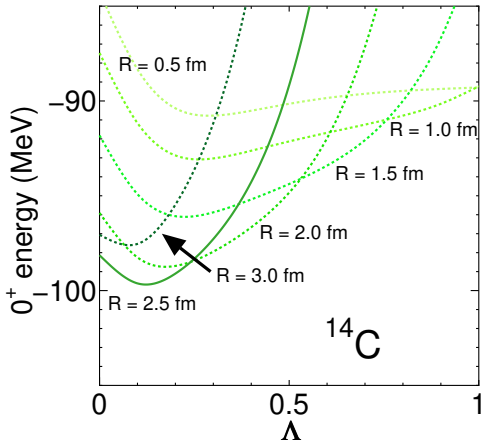

FIG. 7. The R-Λ dependence of the 0^+ energy of ^{14}C for the case of $\nu = 0.22$ fm^{-2}.

V. THE STRUCTURE OF ^{14}C IN THE AQCM APPROACH.

Finally, we discuss ^{14}C itself. In this article we introduced the shell model limit of ^{14}C as a cluster, but we can also discuss this nucleus from the viewpoint of the competition between the components of the α cluster models [6]. In this case the ^{14}C nucleus is described as three quasi α clusters with two valence neutrons. The contribution of the spin-orbit interaction vanishes in the

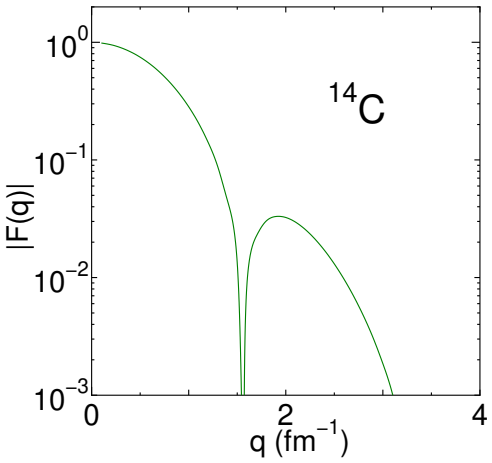

FIG. 8. The elastic form factor for the proton part of the ground state of ^{14}C. The size parameter ν is 0.22 fm^{-2} and Slater determinants with various R and Λ values are superposed based on the GCM.

α cluster models, but the mixing of the shell model components (especially the $(p_{3/2})^6$ configuration for the protons of ^{14}C) can be included by transforming α clusters to quasi clusters. For this purpose, we choose smaller Gaussian wave packets (larger ν parameter $\nu = 0.22$ fm^{-2}) which gives smaller size of the free ^{4}He nucleus. This choice also leads to a more compact size of the ^{14}C nucleus. However, we allow finite distance between the α clusters and superpose different Slater determinants by means of generator coordinate method (GCM). After the GCM calculations, this choice of $\nu = 0.22$ fm^{-2} turns out to be optimal. The resultant radius of ^{14}C after the GCM calculations (2.51 fm) is almost the same as in the previous case (2.55 fm) of shell-model limit ($R = 0.1$ fm, $\Lambda = 1$, and $\nu = 0.17$ fm^{-2}).

Three α clusters with an equilateral triangular shape characterized by relative distance of R form the basis states of the GCM calculations. These states also depend on Λ parameter which introduces the spin-orbit contribution according to Ref. [22] and describes the breaking of the α clusters. Two valence neutrons form a di-neutron cluster and eight neutrons form a tetrahedron shape of four di-neutron clusters. Figure 7 shows the R-Λ dependence of each GCM basis state projected onto 0^+. Because of the size parameter ν which gives a compact ^{4}He, the optimal distance between quasi α clusters becomes a non-zero value. As a result, the combination of $R = 2.5$ fm and $\Lambda = 0.12$ gives the lowest energy of -99.6 MeV. With increasing the R value, the Λ dependence of the 0^+ energy becomes more pronounced. The optimal Λ value of 0.12 at $R = 2.5$ fm looks rather close to zero, but the contribution of the spin-orbit interaction to the total energy is equal to -3.0 MeV. This is not negligible quantity and thus the breaking of the α clusters plays a certain effect. After superposing the Slater determinants with different R and Λ values based

on the GCM, the ground 0^+ state energy is obtained at -100.4 MeV. This corresponds to -19.2 MeV from the $3\alpha+2n$ threshold which compares rather well with experimental value of -20.4 MeV. After the GCM calculations, the contribution of the spin-orbit interaction to the total energy is equal to -3.7 MeV for the ground state. The root mean square (rms) matter radius of the ground state is obtained at 2.51 fm,

The elastic form factor for the proton part is shown in Fig. 8. Note that there is no experimental data for the form factor of ^{14}C. However, the calculated results could be compared with other theoretical results for form factor of ^{12}C (this nucleus has the same proton number as ^{14}C) presented in Refs. [3, 67].

VI. THE STRUCTURE OF ^{28}MG IN THE AQCM APPROACH.

The ^{14}C+^{14}C configuration of ^{28}Mg, which does not have the path to the ground state configuration, has been discussed in Sec. II. The ground state configuration can also be independently prepared based on AQCM employing a treatment similar to that presented in Ref. [23]. In this reference the ground state configuration of ^{28}Si (subclosure configuration of $d_{5/2}$ orbits of the jj-coupling shell model) is described starting from the Brink-type α cluster model.

For the ground state of ^{28}Mg, we introduce the ^{16}O core, which is described with the tetrahedron configuration of four α clusters with small relative distances (0.1 fm); this corresponds to the closed configuration of the p-shell. First, we introduce three α clusters with the equilateral triangular configuration, and next, they are changed into quasi clusters by introducing the imaginary parts for the Gaussian center parameters as in AQCM. Six neutrons in three quasi clusters are transformed into the subclosure configuration of $d_{5/2}$ of the jj-coupling shell model. Remaining two neutrons are put in the center of the system; thus, they are automatically excited to the s-orbits of the sd shell. The number of protons outside ^{16}O is four, so we fill them into two of three quasi clusters introduced for neutrons.

The expectation value of the principal quantum number n of the harmonic oscillator for the 0^+ state of ^{28}Mg is shown in Fig. 9. Here, the ground state configuration is considered as a function of the relative distance between the quasi clusters around ^{16}O. The comparison with the case of ^{14}C+^{14}C configuration shown in Fig. 2 reveals that the n value for the protons is the same (14), but its value for the neutrons is reduced from 24 to 22. The latter is the lowest possible value for 16 neutrons. Unfortunately, the ground state configuration is bound only by 8.75 MeV from the ^{14}C-^{14}C threshold within the present nucleon-nucleon interaction compared with the experimental value of 21.06 MeV with the size parameter fixed to $\nu = 0.17$ fm^{-2}, thus the deviation from the limit of the lowest shell-model configuration would be needed.

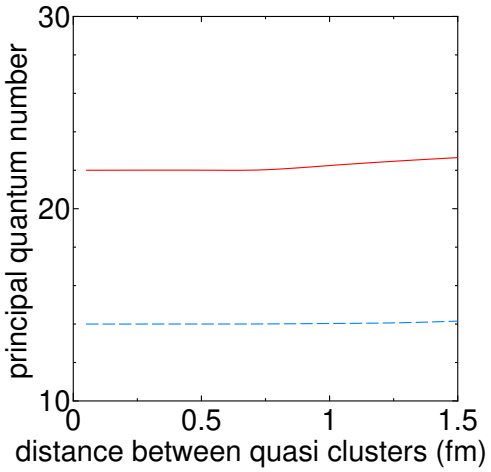

FIG. 9. The expectation value of the principal quantum number n of the harmonic oscillator for the 0^+ state of ^{28}Mg with the ground state configuration considered as a function of the relative distance between the quasi clusters around ^{16}O. Solid red and blue dashed lines are for neutrons and protons, respectively.

VII. CONCLUSIONS

In conclusion, the possibility that ^{14}C can be a building block of cluster structures in medium mass nuclei has been investigated for the first time. On going from light to heavier nuclei, the beta-stability line gradually evolves from $N \sim Z$ to $N \sim 1.3Z$. This suggests that the nuclei with similar neutron to proton ratio can be the building blocks of cluster structures in medium mass nuclei. The ^{14}C nucleus is such a candidate since it has $N/Z = 1.33$. It is strongly bound and reveals itself as a cluster in the ^{14}C emission from actinides. Moreover, the path to the lowest shell-model configuration at short relative distances is closed in the ^{14}C+^{14}C structure, which allows to keep the distance between the clusters approximately equal to 4 fm. Despite underlying differences in theoretical assumptions, the AQCM and CRMF calculations predict the existence of such a cluster structure in ^{28}Mg. It is more pronounced in the AQCM calculations where it survives up to high spin. On the contrary, the rotation leads to washing out of clusterization at spin $I = 16$ in the CRMF calculations. In addition, the possible existence of linear chain ^{14}C+^{14}C+^{14}C cluster structure in ^{42}Ar has been investigated within the framework of the AQCM approach. These results strongly point to an important role of ^{14}C as a building block of cluster structures in medium mass nuclei.

ACKNOWLEDGMENTS

The numerical calculations have been performed using the computer facility of Yukawa Institute for Theoretical Physics, Kyoto University. This work was supported by

KAKENHI Grant Number 17K05440 of Japan, and U.S. Department of Energy, Office of Science, Office of Nuclear Physics under Award No. DE-SC0013037.

[1] D. M. Brink, Proc. Int. School Phys."Enrico Fermi" **XXXVI**, 247 (1966).
[2] M. Freer, H. Horiuchi, Y. Kanada-En'yo, D. Lee, and U.-G. Meißner, Rev. Mod. Phys. **90**, 035004 (2018).
[3] Y. Fujiwara, H. Horiuchi, K. Ikeda, M. Kamimura, K. Katō, Y. Suzuki, and E. Uegaki, Progress of Theoretical Physics Supplement **68**, 29 (1980).
[4] F. Hoyle, Astrophys. J. **1**, 121 (1954).
[5] M. G. Mayer and H. G. Jensen, "Elementary theory of nuclear shell structure", John Wiley, Sons, New York, Chapman, Hall, London (1955).
[6] N. Itagaki, S. Aoyama, S. Okabe, and K. Ikeda, Phys. Rev. C **70**, 054307 (2004).
[7] B. S. Chisholm, D. Erle Nelson, and H. P. Schwarcz, Science (New York, N.Y.) **216**, 1131 (1982).
[8] A. Guglielmetti, D. Faccio, R. Bonetti, S. V. Shishkin, S. P. Tretyakova, S. V. Dmitriev, A. A. Ogloblin, G. A. Pik-Pichak, N. P. van der Meulen, G. F. Steyn, T. N. van der Walt, C. Vermeulen, and D. McGee, Journal of Physics: Conference Series **111**, 012050 (2008).
[9] S. R. Shamami and M. R. Pahlavani, Few-Body Syst **59**, 3 (2018).
[10] M. Gai, M. Ruscev, A. C. Hayes, J. F. Ennis, R. Keddy, E. C. Schloemer, S. M. Sterbenz, and D. A. Bromley, Phys. Rev. Lett. **50**, 239 (1983).
[11] P. Descouvemont and D. Baye, Phys. Rev. C **31**, 2274 (1985).
[12] W. von Oertzen, T. Dorsch, H. G. Bohlen, R. Krücken, T. Faestermann, R. Hertenberger, T. Kokalova, M. Mahgoub, M. Milin, C. Wheldon, and H. F. Wirth, Eur. Phys. J. A **43**, 17 (2010).
[13] W. von Oertzen, M. Milin, T. Dorsch, H. G. Bohlen, R. Krücken, T. Faestermann, R. Hertenberger, T. Kokalova, M. Mahgoub, C. Wheldon, and H. F. Wirth, Eur. Phys. J. A **46**, 345 (2010).
[14] Y. Suzuki, Progress of Theoretical Physics **55**, 1751 (1976), https://academic.oup.com/ptp/article-pdf/55/6/1751/5264825/55-6-1751.pdf.
[15] N. Itagaki, Phys. Rev. C **94**, 064324 (2016).
[16] D. Vretenar, A. V. Afanasjev, G. A. Lalazissis, and P. Ring, Phys. Rep. **409**, 101 (2005).
[17] D. Jenkins, J. Phys. G **43**, 024003 (2016).
[18] N. Itagaki, H. Masui, M. Ito, S. Aoyama, and K. Ikeda, Phys. Rev. C **73**, 034310 (2006).
[19] H. Masui and N. Itagaki, Phys. Rev. C **75**, 054309 (2007).
[20] T. Yoshida, N. Itagaki, and T. Otsuka, Phys. Rev. C **79**, 034308 (2009).
[21] N. Itagaki, J. Cseh, and M. Płoszajczak, Phys. Rev. C **83**, 014302 (2011).
[22] T. Suhara, N. Itagaki, J. Cseh, and M. Płoszajczak, Phys. Rev. C **87**, 054334 (2013).
[23] N. Itagaki, H. Matsuno, and T. Suhara, Progress of Theoretical and Experimental Physics **2016**, 093D01 (2016).
[24] H. Matsuno, N. Itagaki, T. Ichikawa, Y. Yoshida, and Y. Kanada-En'yo, Progress of Theoretical and Experimental Physics **2017**, 063D01 (2017).
[25] H. Matsuno and N. Itagaki, Progress of Theoretical and Experimental Physics **2017**, 123D05 (2017).
[26] N. Itagaki and A. Tohsaki, Phys. Rev. C **97**, 014307 (2018).
[27] N. Itagaki, H. Matsuno, and A. Tohsaki, Phys. Rev. C **98**, 044306 (2018).
[28] A. Tohsaki, Phys. Rev. C **49**, 1814 (1994).
[29] N. Itagaki, A. Ohnishi, and K. Kato, Progress of Theoretical Physics **94**, 1019 (1995).
[30] S. G. Nilsson and I. Ragnarsson, *Shapes and shells in nuclear structure*, (Cambridge University Press, 1995).
[31] R. Tamagaki, Progress of Theoretical Physics **39**, 91 (1968).
[32] S. Ohkubo and K. Yamashita, Phys. Rev. C **66**, 021301 (2002).
[33] M. Kimura and H. Horiuchi, Phys. Rev. C **69**, 051304 (2004).
[34] R. R. Rodríguez-Guzmán, J. L. Egido, and L. M. Robledo, Phys. Rev. C **62**, 054308 (2000).
[35] J. A. Maruhn, M. Kimura, S. Schramm, P.-G. Reinhard, H. Horiuchi, and A. Tohsaki, Phys. Rev. C **74**, 044311 (2006).
[36] D. Ray and A. V. Afanasjev, Phys. Rev. C **94**, 014310 (2016).
[37] J.-P. Ebran, E. Khan, T. Nikšić, and D. Vretenar, Nature **487**, 341 (2012).
[38] J. Maruhn, N. Loebl, N. Itagaki, and M. Kimura, Nuclear Physics A **833**, 1 (2010).
[39] J.-P. Ebran, E. Khan, T. Nikšić, and D. Vretenar, Phys. Rev. C **90**, 054329 (2014).
[40] A. V. Afanasjev and H. Abusara, Phys. Rev. C **97**, 024329 (2018).
[41] S. E. Agbemava, A. V. Afanasjev, D. Ray, and P. Ring, Phys. Rev. C **89**, 054320 (2014).
[42] A. V. Afanasjev and S. E. Agbemava, Phys. Rev. C **93**, 054310 (2016).
[43] E. Ideguchi, D. G. Sarantites, W. Reviol, A. V. Afanasjev, M. Devlin, c. Baktash, R. V. F. Janssens, d. Rudolph, A. Axelsson, M. P. Carpenter, A. Galindo-Uribarri, D. R. LaFosse, T. Lauritsen, F. Lerma, C. J. Lister, P. Reiter, D. Seweryniak, M. Weiszflog, and J. N. Wilson, Phys. Rev. Lett. **87**, 222501 (2001).
[44] A. V. Afanasjev, J. König, and P. Ring, Nucl. Phys. A **608**, 107 (1996).
[45] A. V. Afanasjev, P. Ring, and J. König, Nucl. Phys. **A676**, 196 (2000).
[46] J. L. Egido and L. M. Robledo, Nucl. Phys. A **738**, 31 (2004).
[47] P. Arumugam, B. K. Sharma, S. K. Patra, and R. K. Gupta, Phys. Rev. C **71**, 064308 (2005).
[48] P.-G. Reinhard, J. A. Maruhn, A. S. Umar, and V. E. Oberacker, Phys. Rev. C **83**, 034312 (2011).
[49] J.-P. Ebran, E. Khan, T. Niki, and D. Vretenar, J. Phys. G **44**, 103001 (2017).
[50] A. Afanasjev, EPJ Web Conf. **194**, 06001 (2018).
[51] P. W. Zhao, N. Itagaki, and J. Meng, Phys. Rev. Lett. **115**, 022501 (2015).

[52] J. M. Yao, N. Itagaki, and J. Meng, Phys. Rev. C **90**, 054307 (2014).
[53] T. Ichikawa, J. A. Maruhn, N. Itagaki, and S. Ohkubo, Phys. Rev. Lett. **107**, 112501 (2011).
[54] Y. Iwata, T. Ichikawa, N. Itagaki, J. A. Maruhn, and T. Otsuka, Phys. Rev. C **92**, 011303 (2015).
[55] T. Inakura and S. Mizutori, Phys. Rev. C **98**, 044312 (2018).
[56] G. A. Lalazissis, S. Karatzikos, R. Fossion, D. P. Arteaga, A. V. Afanasjev, and P. Ring, Phys. Lett. **B671**, 36 (2009).
[57] D. G. Jenkins, C. J. Lister, M. P. Carpenter, P. Chowdury, N. J. Hammond, R. V. F. Janssens, T. L. Khoo, T. Lauritsen, D. Seweryniak, T. Davinson, P. J. Woods, A. Jokinen, H. Penttila, F. Haas, and S. Courtin, Phys. Rev. C **86**, 064308 (2012).
[58] A. V. Afanasjev and D. Ray, J. Phys: Conf. Ser. **863**, 012502 (2017).
[59] Y. Taniguchi, Y. Kanada-En'yo, and M. Kimura, Phys. Rev. C **80**, 044316 (2009).
[60] M. Kimura and H. Horiuchi, Phys. Rev. C **69**, 051304 (2004).
[61] Y. Taniguchi, Phys. Rev. C **90**, 054308 (2014).
[62] B. A. Brown, S. E. Massen, and P. E. Hodgson, Journal of Physics G: Nuclear Physics **5**, 1655 (1979).
[63] L. R. Gasques, A. V. Afanasjev, M. Beard, J. Lubian, T. Neff, M. Wiescher, and D. G. Yakovlev, Phys. Rev. C **76**, 045802 (2007).
[64] T. Ichikawa, J. A. Maruhn, N. Itagaki, and S. Ohkubo, Phys. Rev. Lett. **107**, 112501 (2011).
[65] J. M. Yao, N. Itagaki, and J. Meng, Phys. Rev. C **90**, 054307 (2014).
[66] Y. Iwata, T. Ichikawa, N. Itagaki, J. A. Maruhn, and T. Otsuka, Phys. Rev. C **92**, 011303 (2015).
[67] A. Lovato, S. Gandolfi, R. Butler, J. Carlson, E. Lusk, S. C. Pieper, and R. Schiavilla, Phys. Rev. Lett. **111**, 092501 (2013).